Available online at www.sciencedirect.com
SCIENCE DIRECT®
Journal of Colloid and Interface Science 288 (2005) 155–165
JOURNAL OF Colloid and Interface Science
www.elsevier.com/locate/jcis

Phase behavior of block co-poly(ethylene oxide–butylene oxide), $E_{18}B_9$ in water, by small angle neutron scattering ☆

Alexander I. Norman [a,*], Derek L. Ho [b,c], Alamgir Karim [a], Eric J. Amis [a]

[a] *Polymers Division, Stop 8542, National Institute of Standards and Technology, 100 Bureau Drive, Gaithersburg, MD 20899-8542, USA*
[b] *Center for Neutron Research, Stop 8562, National Institute of Standards and Technology, 100 Bureau Drive, Gaithersburg, MD 20899-8562, USA*
[c] *The University of Maryland, College Park, MD 20742, USA*

Received 20 December 2004; accepted 23 February 2005

Available online 31 March 2005

Abstract

We present a small angle neutron scattering (SANS) study into the micellar structures of diblock copolymer $E_{18}B_9$ (where E denotes a ethylene oxide unit and B denotes a butylene oxide unit, 18 and 9 being the number of repeat units respectively) in aqueous solution over a range of five different concentrations (0.2, 1.0, 10.0, 20.0, and 40.0% (by mass fraction)) and eight temperatures (10 to 90 °C). The NG7 30 m SANS instrument provides a q range of 0.0009 to 0.5548 $Å^{-1}$, thus probing the structure over a very broad length scale. At low temperature and low concentration, spherical micelles exist, elongating into worm-like structures at higher temperatures. This transition is observed by the scaling of the scattered intensity at low q and confirmed upon fitting to an appropriate model. Upon increasing concentration, the micelles pack into ordered arrays of either hexagonally packed rod-like micelles or lamellar sheets, again dependent on temperature. Both concentration and temperature effects of this block copolymer have been discussed.
© 2005 Elsevier Inc. All rights reserved.

Keywords: Micelles; SANS; Block copolymers; PDDF; Aqueous

1. Introduction

Over the last decade the micellization and gelation of many poly(oxyalkylene) block copolymers have been studied in great depth and are well documented [1]. In industry, such materials possess many desirable properties and are used widely [2], for example, in oil extraction, burn wound dressings, personal care products, as well as biologically [3], e.g., in bile salts that act as surfactants for the digestion of fats in the body.

E_nP_m block copolymers—where P represents a propylene oxide block, E represents an ethylene oxide block and n and m represent the number of repeat units—have been available for a number of years over a wide range of chain lengths and composition [4]. In 1955 the Wyandotte Chemicals Corporation disclosed the development of the production of ethylene oxide (E)–butylene oxide (B) block copolymers [5]. Commercial introduction of these samples was delayed until 1993 when diblock (E_nB_m) and triblock ($E_nB_mE_n$) copolymers were first marketed by the Dow Chemical Company [6].

Evidence for changes in micelle shape comes from the phase transitions observed by many poly(ethylene oxide)–poly(butylene oxide) block copolymers in aqueous solution, such as the body-centered-cubic (BCC) to hexagonal transition that occurs for $E_{16}B_{10}E_{16}$ [7]. The techniques that elucidate such information include polarized light microscopy, rheology, small angle X-ray scattering (SAXS) and small angle neutron scattering (SANS).

A considerable body of work has been carried out on block copolymers in solution via time resolved scattering

☆ Official contribution of the National Institute of Standards and Technology; not subject to copyright in the United States.

* Corresponding author. Present address: Department of Chemistry and Biochemistry, University of Maryland, College Park, MD 20742-2111, USA.
E-mail address: anorman1@umd.edu (A.I. Norman).

0021-9797/$ – see front matter © 2005 Elsevier Inc. All rights reserved.
doi:10.1016/j.jcis.2005.02.091

techniques (SAXS and SANS) [7–13]. This is a reliable way of determining the mesophase morphology and has been carried out by Fairclough and co-workers [8] for the diblock copolymer $E_{41}B_8$, where a phase diagram was constructed by SAXS measurements that displayed strong agreement with rheological data. It was found that in a region between 24 and 28% (by mass fraction) polymer existed where both face-centered and body-centered cubic structures were observed depending on the temperature. Upon increasing concentration, phase transitions from a BCC phase to hexagonally packed cylinders to lamellae were evident. This has been observed for many block copolymers in many solutions and has been explained in terms of molecular packing and interfacial curvature [14]. Phase transitions of this type are of great interest which will become apparent in this study.

Many publications in the literature [15–17] describe the shape transition within micelles, notably the spherical to elongated micelle transition on increasing temperature, which is of considerable interest to this work. King et al. [15] describe the spherical to rod-like micelle transition at 62 °C for a 1% (by mass fraction) sample of Synperonic P85 ($E_{25}P_{40}E_{25}$), whereas Mortensen et al. [16] modeled the same polymer SANS data to a prolate ellipsoid. As the temperature of the system is increased, the micelles become larger until a characteristic temperature is reached, where the micelle size approaches the size of a fully stretched propylene oxide chain. The micellar structure therefore changes and becomes markedly non-spherical [17].

The process of micellization is entropically driven as stated by Soni et al. [18]. The same block copolymer (Dow notation BM45) was used by Soni as is used in this paper (but of a different batch). SANS was carried out on solutions from 1 to 10% (by mass fraction of polymer) at 30 °C. Micelles were spherical at such temperatures and over the concentration region were of a constant radius (core radius measured at 43 Å). The effect of temperature was explored for a 2% solution. On increasing temperature to 50 °C, a transition from a spherical to ellipsoidal micelle was observed, accompanied by significant changes in micelle size (prolate ellipsoid of dimension 37 × 136 Å) and association number ($N = 318$ for spheres and $N = 743$ for ellipsoids). This effect was attributed to the dehydration of the hydrophilic blocks at elevated temperatures.

The elongation of spherical micelles of ethylene oxide–butylene oxide systems has also been observed by Chaibundit et al. [19,20]. Micellization of $E_{11}B_8$ in water [19] was observed by dynamic light scattering: hydrodynamic radii were obtained at 30 °C (∼60 Å) and 40 °C (∼80–140 Å). The increase in radius also brought about an increase in association number ($N = 63$ at 25 °C and $N = 339$ at 40 °C), characteristic of micelle elongation. The solubilization capacity for drugs (such as Griseofulvin) of such elongated micelles was greater than of spherical micelles. Chaibundit et al. also describe the mesophase behavior and the relation to the spherical and to elongated micelle transition [20]. The diblock copolymer $E_{17}B_{12}$ was shown, by dynamic light scattering, to form elongated micelles. On increasing polymer concentration to 5 wt%, a low modulus gel was observed (at 37 °C). Hard gels were shown to be predominant in concentrations exceeding 25 wt%. Such structures displayed rich rheological properties. Rheology and polarized light microscopy were used to estimate the mesophase morphology. A birefringent gel, attributed to grains of elongated aligned micelles, was observed at room temperature for such hard gels. High temperature gels were also shown to persist at temperatures exceeding 70 °C. Such gels were shown to be isotropic by polarized light microscopy. Rheology measured a storage modulus exceeding 1 kPa. It was speculated that this phase was of an ordered cubic structure. The formation of such a phase was reportedly due to scission of cylindrical micelles at elevated temperatures.

Recently, Hamley et al. [21] confirmed the transition between spherical and elongated micelles in a 1% solution (by mass fraction) of diblock copolymer $E_{18}B_{10}$. This was performed via SANS techniques over a temperature range 20–60 °C. This is consistent with the observation of hexagonally packed rod-like micelles for the same block copolymer in more concentrated solution [22].

In this work, the technique of SANS is used to explore this phenomenon in the same block copolymer. The block copolymer, available from Dow Chemicals and denoted BM45-1600, is from a separate batch and of architecture $E_{18}B_9$. Small differences in composition will occur from batch to batch but as one would expect, since the B block is only one unit shorter, the behavior in aqueous solution should prove to be remarkably similar. Existing work shows the elongation of such micelle structures. We attempt to reproduce such s phenomenon and further prove, not only by SANS data alone, but also by performing an inverse Fourier transformation on the SANS data, to yield the pair distance distribution function, $p(r)$. Our SANS data is recorded over a wider concentration and temperature window, therefore consequences of micelle elongation on the mesophase formation are investigated. As described in the experimental section, SANS data is collected over a broader q range than that described by Hamley et al. [21], thus gaining insight into information at larger length scales.

2. Materials and methods

2.1. Synthesis and characterization of polymers

The diblock copolymer $E_{18}B_9$ was obtained as a gift from Dow Chemicals and was given the notation BM45-1600. To compare the results with previous studies on this polymer, the material was used as received and not purified further. Other batches used of this same material have been quoted as $E_{18}B_{10}$ [21] and $E_{17}B_{12}$ [20]. Such materials are synthesized by sequential anionic polymerization of 1,2-butylene oxide and ethylene oxide. Further details of the synthesis of similar diblock copolymers (such as E_6B_{11}, which forms multil-

amellar vesicles in aqueous solution) have been described elsewhere [23]. The composition was determined by nuclear magnetic resonance (NMR) spectroscopy using methods described previously [24].

2.2. Micelle preparation

Neat block copolymer was added to deuterated water, D_2O, until the desired concentration was reached. The sample vial was shaken by hand for approximately 60 s. Aqueous dispersions were prepared in 0.2, 1.0, 10.0, 20.0, and 40.0% by mass fraction concentrations. Samples were allowed to stand for a minimum of 48 h before any analysis was performed.

2.3. Small angle neutron scattering measurements

SANS experiments over the q range from 0.0009 to 0.5548 $Å^{-1}$ were carried out using the NG7 30-m SANS instrument at the National Institute of Standards and Technology (NIST) Center for Neutron Research (NCNR), Gaithersburg, MD [25].

Three instrumental settings were used to cover the range of the scattering vector, q, where $q = (4\pi \sin\theta)/\lambda$, 2θ being the scattering angle and λ the neutron wavelength. The three settings (wavelength and sample-to-detector distance) used to achieve this q range are 8.09 Å and 15.3 m (with the focusing lens configuration [26]), 6.0 Å and 6.0 m, and 6.0 Å and 1.1 m with a wavelength resolution of $\Delta\lambda/\lambda = 0.11$. The scattered intensity was corrected for background and parasitic scattering, placed on an absolute level using a calibrated secondary standard and circularly averaged to yield the scattered intensity, $I(q)$, as a function of the wave vector, q. Finally the low incoherent background scattering was estimated. This was determined from the asymptotic slopes of $I(q)q^4$ vs q^4 [27] and subtracted from each data set.

The samples were dissolved in D_2O to provide a low incoherent background and strong contrast. Samples were loaded into quartz cells of 1 mm path length. The five samples prepared were investigated at temperatures of 10, 20, 30, 40, 50, 65, 80, and 90 °C. Due to time constraints not all samples were probed at such a low q range, giving a q range of 0.0053 to 0.5548 $Å^{-1}$ for some of the samples studied. Table 1 lists each the temperature and the q range studied for each concentration of block copolymer. The low concentration samples (0.2 and 1.0%) were at such a concentration where structure factor effects can be neglected and the SANS experiment probes the single particle form factor which is a function describing the shape of the non-interacting individual micelles. This is discussed in greater detail in the proceeding section. Samples at higher concentration (10.0, 20.0 and 40.0%) were studied to observe the possibility of the formation of lyotropic liquid crystalline phases. The error (standard uncertainty) associated with the SANS experiments is dependent on various factors, such as the detector count rate, the estimation in conversion of pixel number to scattering vector, and the secondary standard. For clarification purposes, the error bars in some of the figures have been omitted.

Table 1
Temperature and q range investigated for each block copolymer concentration

Concentration (wt%)	Temperature (°C)	q range ($Å^{-1}$)
0.2	10–40, 65, 90	0.0065 q 0.5548
	50, 80	0.0009 q 0.5548
1.0	10, 30, 50, 80	0.0009 q 0.5548
	20, 40, 65, 90	0.0065 q 0.5548
10	10–90	0.0065 q 0.5548
20	10–90	0.0065 q 0.5548
40	10, 30, 50, 80	0.0009 q 0.5548
	20, 40, 65, 90	0.0065 q 0.5548

3. Theory and data analysis

For a system of particles the scattered intensity is given as

$$I(q) = n\Delta\rho^2 V^2 P(q) S(q), \tag{1}$$

where n is the number density of the particles, $\Delta\rho$ is the difference in scattering length density, V is the volume of particles, $P(q)$ is the form factor, and $S(q)$ is the structure factor, with the wavenumber, $q = (4\pi \sin\theta)/\lambda$ (θ is the angle between the scattered and incident beam and λ is the wavelength of the incident radiation).

The form factor is a function which describes the intraparticle scattering from the *shape* of the scattering particles. The structure factor is a function which describes the interparticle scattering due to the *interactions* of the scattering particles. The spatial correlations arising in the structure factor are due to the radial distribution function, $g(r)$, which is related to the probability of finding the center of any particle at a distance r from the center of a given particle. For N particles in a volume V at a distance r from any given particle, the structure factor is defined as [29]

$$S(q) = 1 + 4\pi \frac{N}{V} \int_0^\infty g(r) - 1 \; r^2 \frac{\sin(qr)}{qr} \, \mathrm{d}r. \tag{2}$$

The structure factor, $S(q)$, given in Eq. (2) is neglected in many data sets throughout this paper since the concentration is extremely low, hence $I(q)$ follows the form factor which was modeled depending on the *shape* of the scattered particles, described below.

3.1. Micelle shape analysis

We can understand the SANS profiles, such as that illustrated in Fig. 1, of such systems by concentrating on three separate regions. At low q, the behavior of $I(q)$ is general and independent of the shape of the scattering particle. This

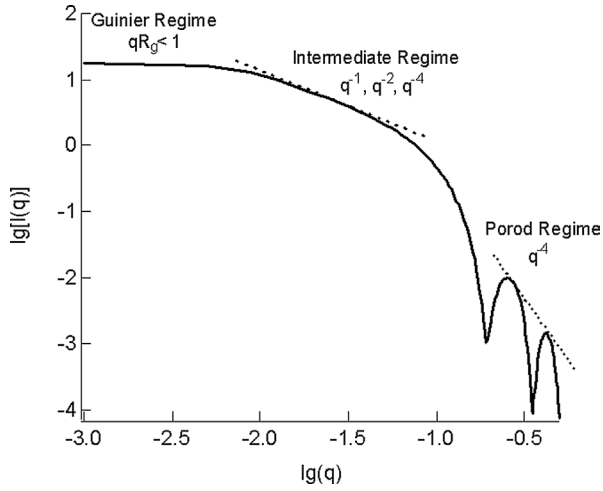

Fig. 1. Generalized small angle scattering profile showing the different regimes which reflect different decays of intensity in scattering vector, q.

is because at small q values (qR_g 1) the spatial resolution is not sufficient to elucidate particle shape and only information regarding dimension can be obtained. In this case $I(q)$ is described by the Guinier relation [28]

$$I(q) = I(0)\exp\ -q^2R_g^2/3\ , \tag{3}$$

where R_g is the radius of gyration of the particle and $I(0)$ is the scattered intensity at $q = 0$, which is determined from the double logarithm plot:

$$\ln\ I(q)\ = \ln\ I(0)\ - \frac{q^2R_g^2}{3}. \tag{4}$$

Since the data shown is in absolute scale, $I(q)$ being expressed in units of cm^{-1}, we can make use of $I(0)$, which is calculated by the y-intercept of a Guinier plot as expressed in Eq. (4), to determine the aggregation number, which is defined as the number of molecules that are within the micelle. The aggregation number, n_{agg}, is determined from

$$I(0) = n_{\mathrm{agg}}\phi_{\mathrm{polymer}}K_nV_i, \tag{5}$$

where the neutron contrast factor $K_n = \Delta\rho^2N_A$ and $\Delta\rho = \rho_i - \rho_j = (b_i/v_i - b_j/v_j)$. N_A is Avogadro's constant (6.023×10^{23} molecules/mol), ϕ_{polymer} is the concentration of polymer, V_i is the specific volume of species i in units of cm^3/mol, and $\Delta\rho^2$ is the square of the difference in scattering length density ($\mathrm{mol}^2/\mathrm{cm}^4$) between polymer ($i$) and solvent ($j$). b is defined as the scattering length in cm.

The high q region of the SANS profile describes the Porod regime where the spatial resolution is very good. This enables the observation of the interface between particle and solvent. Here, the intensity typically scales as q^{-4} [29]. Polydispersity in the size and the shape of the scattered particles will affect this scaling due to a broader interface between scattered particles and surrounding solvent.

The intermediate range of the profile is the region in which the form factor contains information regarding particle size and shape. In this region the scaling of $I(q)$ results from the dimensionality of the scattered particle, for example, the scattered intensity of a rod-like micelle scales as q^{-1}, whereas a vesicle shell or a disk scales as q^{-2} [30].

Further micelle shape determination is achieved using the generalized indirect Fourier transformation (GIFT) method [31]. The conventional Fourier transformation of $I(q)$ involves the integral

$$p(r) = \frac{1}{2\pi^2}\int_0^\infty I(q)qr\sin(qr)\,\mathrm{d}q, \tag{6}$$

which yields the pair distance distribution function $p(r)$, where r is the distance in real space. This function can be used to determine size, shape and internal structure of scattered particles with high accuracy in the size range of approximately 10 to 1000 Å (depending on the q range of the instrument used to collect the data). The $p(r)$ function can be understood as follows. The scattered particle is divided into many small volume elements (small in comparison to local density fluctuations). The $p(r)$ function is proportional to the product of the different scattering lengths n_in_k of two volume elements i and k with a center-to-center distance between r and $r + \mathrm{d}r$. Similarly, the height of the $p(r)$ function is proportional to the number of such scattering lengths that are found inside the particle within the interval r to $r + \mathrm{d}r$ [31]. The direct calculation of $p(r)$ using Eq. (6) requires scattering data in the full q range from 0 to ∞. The limited q range available experimentally will lead to strong oscillations in $p(r)$. These effects have been minimized in a new data analysis technique using the indirect Fourier transformation [31–33]. This method performs desmearing and Fourier transformation simultaneously, assuming that $p(r) = 0$ for $r > D_{\max}$, where $D_{\max}$ is the maximum particle dimension.

The form factor arising from the scattering of monodisperse, non-interacting hard spheres is shown in the equation [31]

$$P(q) = \left[\frac{3[\sin(qR) - qR\cos(qR)]}{(qR)^3}\right]^2, \tag{7}$$

where R is the radius of the scattered particle.

Fig. 2 shows our SANS data with the respective fit to Eq. (7) for 0.2 and 1.0% at 10 °C.

The non-interacting spherical model (which does not take into account polydispersity) fits the data well over the q range probed. The oscillations at higher q values are smeared out due to polydispersity effects. The scaling of $I(q)$ at low q is q^0, describing the Guinier region of the curve, indicating that no large particles are present, such as worm-like micelles that may possibly mask the Guinier region at the lowest accessible q range, or any inter-particle interactions arising from $S(q)$ contributions. The radii obtained were 58.0 ± 1 Å for 0.2%. Fig. 2 also shows the SANS data and the fit to a spherical model for 1%. The significant upturn in $I(q)$ at low q is over a q range lower than that probed for the data shown for 0.2%. The fit to the spherical

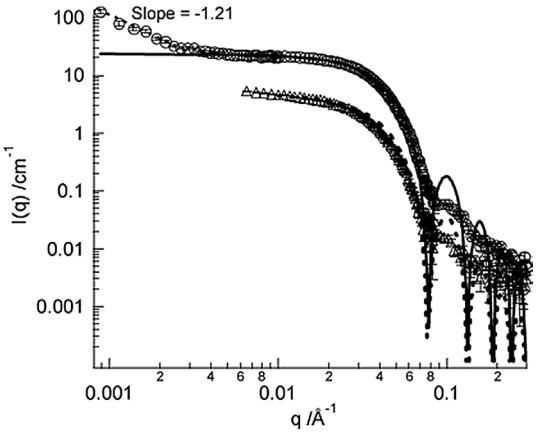

Fig. 2. SANS intensity profiles, with respective fits to a monodisperse non-interacting sphere, for 0.2% by mass fraction (open triangles, data; solid line, fit) and 1.0% by mass fraction (open circles, data; broken line, fit) $EO_{18}BO_9$ in D_2O at 10 °C. The lines show the fit to Eq. (3); a hard sphere model with no polydispersity.

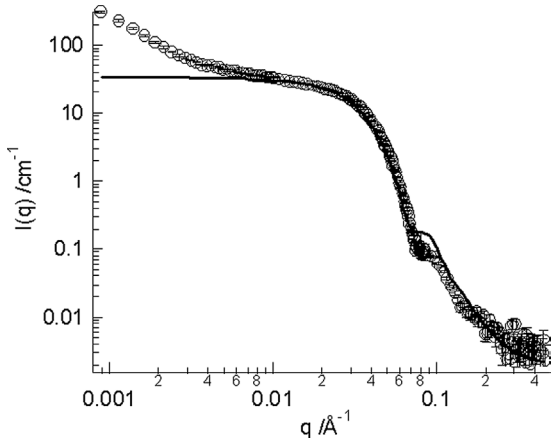

Fig. 4. SANS intensity profile from a solution of 1.0% by mass fraction of $EO_{18}BO_9$ at 50 °C. The solid line indicates the fit to the model describing polydisperse hard spheres.

Fig. 3. SANS intensity profiles from a solution of 0.2% by mass fraction of $EO_{18}BO_9$ at 20 °C. The solid line indicates the fit to a hard sphere with polydispersity. Inset shows the Guinier plot, $\ln q = \ln[I(0)] - q^2 R_g^2/3$, where $y = 1.9266 - 1045x$.

model works well for 1% over the same q range as that for 0.2%. This model also yields a radius of 58.0 ± 1 Å for 1.0%. The change in slope at very low q ($I(q)$ scales as $q^{-1.21}$ rather than zero) observed for 1.0% may be attributed to a weak interaction of micelles that have formed an aggregate which is beyond the size range detectable by the conventional SANS setup.

The introduction of polydispersity into this model is illustrated in Fig. 3, which shows SANS data and the respective fit for a 0.2% polymer solution at 20 °C. The monodisperse model was used in Fig. 2 for illustrative purposes only, data was fitted using the polydisperse model, and the same R value was obtained (which is summarized in Table 2). This function [31] calculates the scattered intensity for a population of polydisperse spheres including hard sphere interactions between the particles. A Schultz distribution [34] is used to describe the polydispersity, p, of the diameter, $p = s/R$, where s^2 is the variance of the distribution and R is the mean particle radius. We can see how the introduction of polydispersity smears out the high q oscillations in $P(q)$ by comparing Figs. 2 and 3. At low temperatures the intensity, $I(q)$, scales as $q^{-0.4}$ over the q range 0.007 to 0.02 Å^{-1}. This deviation from the Guinier regime has been attributed to polydispersity in size of scattering elements. However, other possible explanations are the elongation of the spherical particles into oblate or prolate ellipsoids. In this study the fit to a polydisperse spherical model proved more accurate than the fit for an ellipsoid. The inset to Fig. 3 shows the Guinier plot, which is performed to extract $I(0)$ which is used, in our case to determine the aggregation number.

The effect of increasing the concentration five-fold, to 1 wt% polymer at 20 °C, is shown in Fig. 4. The fit to a polydisperse hard sphere gives a radius of 54 ± 1 Å with a polydispersity of 15%. Once again, we see the deviation from the scaling of q^0 in intensity at the lowest q range, which we assume is due to aggregation effects as described above.

The second model we shall discuss is that of a prolate ellipsoid. A prolate ellipsoid is needle-like in shape, as opposed to an oblate ellipsoid, which is disk-like and has a very different scattering profile. For the prolate ellipsoid the form factor is described [35],

$$P(q) = \int_0^1 f^2\left(qr_b\left(1 + x^2(\nu^2 - 1)\right)^{1/2}\right) dx, \tag{8}$$

$$f(z) = 3V_{\text{ell}}\frac{(\sin z - z\cos z)}{z^3}, \tag{9}$$

$$V_{\text{ell}} = \frac{4}{3}\pi r_a r_b^2, \qquad \nu = \frac{r_a}{r_b}, \tag{10}$$

where $f(z)$ is the scattering amplitude and $z = qr_b\{1 + x^2(\nu^2 - 1)\}^{1/2}$, r_a is the short axis of the ellipsoid, r_b is the long axis, ν is the ratio of the short axis to the long axis, $x = R_g^2 q^2$ (R_g is the radius of gyration), and V is the volume of the ellipsoid.

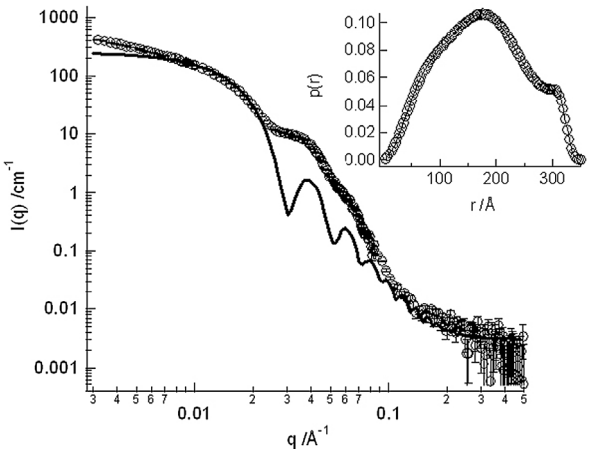

Fig. 5. SANS intensity profile from a solution of 1.0% by mass fraction of $EO_{18}BO_9$ at 50 °C. The solid line indicates the fit to a prolate ellipsoid. The inset shows the pair distance distribution function.

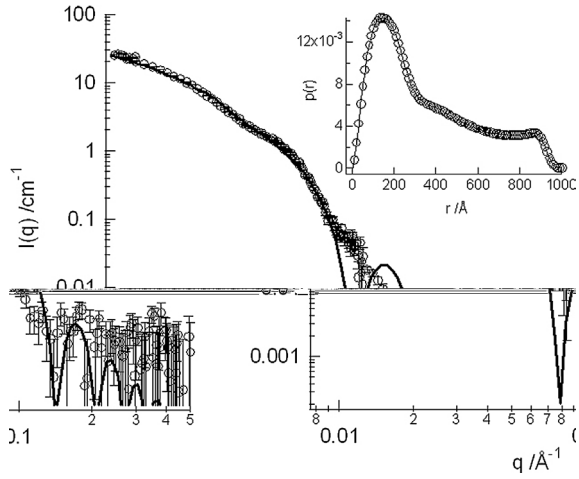

Fig. 6. SANS intensity profile from a solution of 0.2% by mass fraction of $EO_{18}BO_9$ at 50 °C. The solid line indicates the fit to a semi-flexible chain with excluded volume. The inset shows the pair distance distribution function.

On increasing temperature, the observation of an increased aggregation number is evident (we refer the reader to Table 2 for a summary of all data) along with the upturn in $I(q)$ at low q, suggesting the elongation of these spherical micelles into elongated structures. Fig. 5 shows the SANS data for 1.0 wt% polymer at 50 °C and the fit to the model for a prolate ellipsoid. Polydispersity effects are not included in this model, which explains why the oscillations at larger q values are so well defined in comparison to the data. A broad peak observed at 0.045 $Å^{-1}$ arises from form factor contributions due to the micellar radius. The model gives a long axis of 250 ± 10 Å and a short axis of 130 ± 10 Å. The inset to Fig. 5 displays the $p(r)$. This function is not perfectly symmetric and is characteristic of an elongated structure.

Finally, a model for semi-flexible chains with excluded volume [36] is fitted to the data which describes non-rigid, elongated micelles, which we will refer to as "worm-like" micelles. Such structures can be estimated from the scaling of $I(q)$ at low q. The scattered intensity observed in this system scales as $q^{-5/3}$ [36], which is intermediate of the scaling law for rigid rods (q^{-1}) and Gaussian coils (q^{-2}). This suggests that the micelles are not rigid; they do possess some flexibility and are worm-like in shape.

The worm-like model, which is a non-linear least squares fit of the scattered intensity for semi-flexible chains with excluded volume, can be described as the following. Consider a polymer of N units. When diluted in a solvent the polymer gets entangled as a result of the chain flexibility. The motion of the chains can be modeled by the random walk model [36] that describes the features of the polymer configurations and diffusive motion. The length of such a walk is given as $\langle R^2 \rangle = aN^{1/2}$, where a is a given length. In good solvents (such as water for polymers in this study), the polymer coil behaves as a self-avoiding random walk (the walk has an additional restriction in that it cannot cross itself within a given distance, a). This concept is known as the excluded volume effect and is a part of the worm-like micelle model used in these subsequent calculations. The Kuhn length, b, which is considered as rigid segments behaving independently over the whole chain, can characterize the stiffness of the chain. Hence in a semi-flexible chain of contour length, L, there are L/b segments. Values of the Kuhn length appear in the intermediate region of the SANS curve that can be used to describe the chain flexibility. Further details of this model can be found in Pedersen and Schurtenberger [36] and references therein. Further evidence to suggest this worm-like shape comes from the pair distance distribution function, PDDF, or $p(r)$.

An example of a fit to this model is shown in Fig. 6. Fig. 6 shows the SANS data at 50 °C for 0.2 wt% polymer. The model gives fitted parameters, $R = 49 \pm 1$ Å, $b = 145 \pm 10$ Å, and $L = 950 \pm 10$ Å. The inset displays the $p(r)$ function. This is typical of elongated structures due to the asymmetry shown. Ripples appearing at larger values of r are characteristic of axial inhomogeneity along the cylinder, which is present if such structures, and possess some degree of flexibility. The point at which the $p(r)$ falls to zero is indicative of the particles maximum dimension, which is 1000 Å, in good agreement with the fit to the worm-like model in $I(q)$. Such transitions observed from spherical to ellipsoidal to "worm-like" micelles will be discussed in the next section.

The subsequent fitted parameters for 0.2 and 1.0 wt% (at all temperatures investigated) are shown in Table 2 for all models used.

3.2. Consequences of micelle shape on mesophase behavior

The structure factor, $S(q)$, is a relevant parameter to the observed scattered intensity as the concentration increases to 10 wt%. Correlation peaks shown in $I(q)$ are apparent, indicating the ordering of micelles into lyotropic liquid crystalline phases.